Published in final edited form as:
Acta Biomater. 2013 June ; 9(6): 6905–6914. doi:10.1016/j.actbio.2013.02.008.

Controlled delivery of mesenchymal stem cells and growth factors using a nanofiber scaffold for tendon repair

CN Manning[a], **AG Schwartz**[a], **W Liu**[b], **J Xie**[c], **N Havlioglu**[d], **SE Sakiyama-Elbert**[c], **MJ Silva**[a], **Y Xia**[e,*], **RH Gelberman**[a,*], and **S Thomopoulos**[a,*]

[a]Department of Orthopaedic Surgery, Washington University, St Louis, MO

[b]Department of Chemical & Biomolecular Engineering, Georgia Institute of Technology, Atlanta, GA

[c]Department of Biomedical Engineering, Washington University, St Louis, MO

[d]Department of Pathology, St Louis University Hospital, St Louis, MO

[e]Department of Biomedical Engineering, Georgia Institute of Technology, Atlanta, GA

Abstract

Outcomes after tendon repair are often unsatisfactory, despite improvements in surgical techniques and rehabilitation methods. Recent studies aimed at enhancing repair have targeted the paucicellular nature of tendon for enhancing repair; however, most approaches for delivering growth factors and cells have not been designed for dense connective tissues such as tendon. Therefore, we developed a scaffold capable of delivering growth factors and cells in a surgically manageable form for tendon repair. The growth factor PDGF-BB along with adipose-derived mesenchymal stem cells (ASCs) was incorporated into a heparin/fibrin-based delivery system (HBDS). This hydrogel was then layered with an electrospun nanofiber poly-lactic-co-glycolic acid (PLGA) backbone. The HBDS allowed for the concurrent delivery of PDGF-BB and ASCs in a controlled manner, while the PLGA backbone provided structural integrity for surgical handling and tendon implantation. *In vitro* studies verified that the cells remained viable, and that sustained growth factor release was achieved. *In vivo* studies in a large animal tendon model verified that the approach was clinically relevant, and that the cells remained viable in the tendon repair environment. Only a mild immunoresponse was seen at dissection, histologically, and at the mRNA level; fluorescently-labeled ASCs and the scaffold were found at the repair site 9 days postoperatively; and increased total DNA was observed in ASC-treated tendons. The novel layered scaffold has the potential for improving tendon healing due to its ability to deliver both cells and growth factors simultaneously in a surgically convenient manner.

Keywords

sustained delivery system; electrospinning; stem cells; tissue engineering; intrasynovial flexor tendon

Corresponding Authors Contact information: Stavros Thomopoulos, Washington University, 660 South Euclid Campus Box 8233, St Louis, MO 63110, Phone: 314-362-8605, Fax: 314-362-0334, ThomopoulosS@wudosis.wustl.edu.
*Study design, *in vitro* studies, *in vivo* studies: Stavros Thomopoulos, Ph.D. Clinical relevance and surgical methods: Richard H. Gelberman, M.D. Scaffold development: Younan Xia, Ph.D.
Dr. Xie is currently at Marshall Institute for Interdisciplinary Research and Center for Diagnostic Nanosystems, Marshall University, Huntington, WV

1. INTRODUCTION

Hand and wrist injuries account for nearly 1 in 5 emergency room patient visits and rank as the most expensive injury types when health care costs and productivity losses were accounted for (more expensive than knee and lower limb fractures, hip fractures, and skull-brain injury) [1]. Many of these injuries are debilitating and require extensive tendon surgical repair [2-4]. Despite advances in suture and rehabilitation methods over the past three decades, tendon repair outcomes are highly variable. Cell-based and growth factor-based therapies can fundamentally change the clinical approach to tendon repair. Recent attempts to improve tendon healing have focused on applying growth factors to increase cell proliferation and matrix synthesis [5-13]. However, because there are typically few cells at the repair site, growth factor-stimulated increases in biological activity have not been sufficient to improve the strength or stiffness of the repair [6, 9]. A novel strategy to improve these outcomes is to combine the delivery of growth factors with autologous stem cells at the time of surgical repair (Figure 1). Therefore, our objective in the current study was to develop a scaffold for tendon repair applications that is capable of controlled delivery of cells and growth factors.

This scaffold design must take into consideration surgical handling and repair-site implantation requirements. Previously, a fibrin/HBDS was used to deliver various growth factors at the time of tendon injury and repair [6-10, 14]. The hydrogel consistency of the scaffold, however, made it difficult to handle, surgically implant, and retain at the injury site. Therefore, a new scaffold is presented herein that combines the previous HBDS with an aligned electrospun nanofiber PLGA backbone. The scaffold consists of eleven alternating layers of PLGA nanofiber mats and HBDS (i.e., 6 layers of PLGA and 5 layers of fibrin). The scaffold allows for the delivery of cells and growth factors in a controlled manner [7, 8, 10, 15], while the PLGA backbone provides a structure that mimics collagen fiber diameter and alignment in tendon and enhances the surgical handling properties of the scaffold. While natural matrices (e.g. collagen, fibrin) are advantageous in terms of biocompatibility, polymers (e.g. PLGA) provide better control of degradation and mechanical properties. PLGA was chosen because it is biodegradable, has the appropriate mechanical properties, can easily be electrospun, and is FDA approved [16, 17]. PLGA polymer nanofiber mats are biodegradable in an aqueous environment but are resistant to enzymatic degradation. The ratio of lactic to glycolic monomers can be varied to alter the degradation rate and mechanical properties.

A cell source appropriate for tenogenesis should be used in efforts to enhance tendon repair. Most previous efforts to apply cell-based therapies to tendon repair have used bone marrow-derived stem cells, and little attention has been given to ASCs. ASCs may be an attractive cell source from a translational standpoint. Compared to bone marrow-derived stem cells, ASCs can be harvested with less invasive procedures [18, 19], are available in more abundant quantities [18, 19], demonstrate comparable immunosuppressive capabilities, and demonstrate equivalent potential to be differentiated along multiple mesenchymal lineages [20-23]. Specifically, treatment of ASCs with growth differentiation factor 5 (GDF5, also known as bone morphogenetic protein 14) has been shown to drive tenogenesis of the ASCs, as evidenced by an upregulation of the gene expression of multiple tenogenic markers [24, 25]. The use of autologous ASCs expanded for seven days or less for tendon repair represents a promising new direction in treatment and is amenable to the common clinical practice of performing suture repair several days to three weeks after a flexor tendon injury.

In the current study, we present a novel scaffold for use in tendon repair. The ability of the scaffold to maintain cell viability and deliver growth factors is demonstrated *in vitro*. Scaffold biocompatibility, feasibility for use in tendon repair, and post-implantation cell

viability are demonstrated *in vivo* using a clinically relevant large animal model of flexor tendon injury and repair. In this study, our aims were to show that: (1) controlled delivery of cells and growth factors can be achieved from the scaffold, (2) the scaffold can be implanted successfully at a flexor tendon repair site *in vivo*, and (3) the scaffold is biocompatible *in vivo*.

2. METHODS

2.1 HBDS/Nanofiber layered scaffold fabrication

The HBDS/nanofiber scaffold consisted of eleven alternating layers of aligned electrospun PLGA nanofiber mats and HBDS (i.e. 6 layers of PLGA and 5 layers of fibrin, Figure 2). PLGA was chosen because of its biodegradability and mechanical properties [16, 17, 26]. The electrospinning solution was prepared at a concentration of 0.25 g/mL by dissolving PLGA (85:15, MW 50,000-75,000, Sigma Aldrich) in a mixture of dichloromethane (DCM) and dimethylformamide (DMF) at a ratio of 4:1. The solution was loaded into a plastic syringe equipped with a stainless steel needle (23-gauge) connected to a high-voltage supply (ES30P-5W, Gamma High Voltage Research). The feed rate was set at 0.5 mL/h, controlled by a syringe pump (KDS-200, Stoelting). Fibers with diameters of 400-700 nm (similar in size to collagen fibrils in tendon) were collected on a custom-made rotating mandrel to create a uniaxial array of nanofibers designed to mimic the anisotropic extracellular matrix of tendon tissue (Figure 2B inset) [27, 28]. After 2.5 h of electrospinning, the polymer nanofiber mat (~100 micrometers) was released from the collector and freeze-dried for 72 hr to remove residual solvents. Scanning electron microscope images (SEM, FEI Nova 200 Nanolab, accelerating voltage 5kV, 3500X) of representative scaffolds were used to calculate the approximate diameter and orientation of the fibers. The nanofiber mats were then sterilized with ultraviolet light for 30 min (Thermo Scientific, model 1375, wavelength 253.7nm, power 40W) and cut into 3×7 mm pieces (with the fibers aligned in the 7 mm direction).

The HBDS included a bi-domain peptide with a factor XIIIa substrate derived from α_2-plasmin inhibitor at the N-terminus and a C-terminal heparin-binding domain from anti-thrombin II [6-10, 15]. The bi-domain peptide was covalently cross-linked to fibrin during polymerization by the transglutaminase activity of factor XIIIa. The peptide immobilizes heparin electrostatically to the matrix, which in turn immobilizes heparin-binding growth factors, preventing their diffusion from the matrix. Fibrin matrices (30μl total) were made with the following final component concentrations: 10 mg/mL of human fibrinogen concentration (20 mg/ml stock solution, EMD Bio), 6.9 mM of $CaCl_2$ (50mM stock solution), 12.5 units/mL of thrombin (1000U/ml stock solution), 1.6 mg/ml peptide (25mg/ml stock solution) with sequence dLNQEQVSPK(βA)FAKLAARLYRKA-NH_2 (where dL denotes dansyl leucine), and 1.2 mg/ml heparin (45 mg/ml stock solution, Sigma, H-9399) in Tris-buffered saline (TBS) (137 mM NaCl, 2.7 mM KCl, 33 mM Tris; pH, 7.4). The fibrin/HBDS was polymerized directly onto the PLGA nanofiber mats (one layer at a time, 6 μL per layer), effectively serving as a bond between layers. Once fibrin and thrombin were mixed together, the fibrin/HBDS layer began to polymerize within 30 s and reached a gel-like consistency within 1-2 min. The nanofiber mat was placed on top of the fibrin/HBDS after the fibrin/HBDS reached a gel-like consistency. This process was repeated to build a scaffold with the appropriate number of layers. The assembly of each scaffold in this study was completed in ~15 minutes. The assembled scaffold was then left in the incubator (37°C, 5%CO_2, 95% humidity) for ~1 hr to allow for complete fibrin/HBDS polymerization and full adherence between the fibrin/HBDS and the nanofiber mat layers. For cellular scaffolds, 1×10^6 ASCs (per scaffold, 3.3×10^4 cells/μL) were incorporated into the fibrinogen solution prior to polymerization. Similarly, heparin-binding growth factors (e.g., platelet derived growth factor BB (PDGF-BB)) were integrated into the fibrinogen solution prior to

polymerization, as described in subsequent sections. The final dimensions of the scaffolds were 7×3×1 mm (Figure 3E).

2.2 Cell isolation and culture

ASCs were isolated 1-2 weeks prior to use. Adipose tissue from the abdominal cavity of canines (N=8) was removed surgically. To harvest adipose tissue, dogs were sedated and a 2-4 cm skin incision was made in the caudal abdomen just below the umbilicus exposing the subcutaneous fat lying lateral to the midline. A 10-15 g sample of adipose tissue was isolated and excised bilaterally and the skin wound was closed. The adipose tissue was minced and digested in 0.2% Collagenase A in phosphate-buffered saline (PBS) for 2 h, collected, and centrifuged for 10 minutes at 12,000 rpm. The digested tissue was filtered using a cell strainer and pelleted by centrifugation. The supernatant was aspirated and the pelleted cells were resuspended in alpha-modified eagles medium (alpha-MEM) with 10% fetal bovine serum (FBS) and 1 % penicillin/streptomycin and cultured for 1-2 weeks (37°C, 5% CO_2, 100% humidity). The cells were used between passages 2-4. Numerous investigators, using similar isolation methods, have described the resultant cell population as mesenchymal stem cells based on surface markers (via FACS) and pluripotency [22, 23, 29, 30]. The cells in the current study demonstrated pluripotency based on standard adipogenic, osteogenic, chonodrogenic, and tenogenic protocols (data not shown).

2.3 In vitro studies

2.3.1 Cell culture—A set of scaffolds was fabricated for *in vitro* time-zero imaging in order to visualize the different components of the constructs (Figure 2). These scaffolds contained fluorescein isothiocyanate (FITC)-labeled PLGA, Alexa Fluor 546-labeled fibrinogen (Invitrogen Corporation, CA), and ASCs labeled with Hoechst 33258 (Invitrogen Corporation, CA). A series of *in vitro* experiments were also performed to: (1) assess the viability and proliferation of ASCs within the scaffold, and (2) determine growth factor release kinetics from the HBDS/nanofiber scaffold.

2.3.2 Cell viability—To assess the viability and proliferation of ASCs within the scaffold, a set of HBDS/nanofiber scaffolds containing 1×10^6 ASCs were fabricated (N=4 cell isolations, 20 scaffolds total) and cultured in 24 well plates for up to 14 days. The scaffolds were given fresh phenol-free alpha-MEM containing 10% FBS and 1% penicillin/ streptomycin daily. At each sacrificial time point (0, 3, 7, 11, and 14 days) the scaffolds were delaminated with forceps (i.e., the individual layers of the scaffold were separated from each other) and a Vybrant 3-(4,5-Dimethylthiazol-2-yl)-2,5-diphenyltetrazolium bromide (MTT) Cell Proliferation Assay (Invitrogen Corporation, CA) was performed according to the manufacturer's instructions. Live cells reduced the MTT solution to a purple formazan product, which was solubilized with 200μl of 2-Propanol. The absorbance of the solubilized formazan was measured using a microplate reader at 470 nm. The relative number of live cells within the scaffold was determined by averaging the absorbance values of four different cell isolations at each timepoint and normalizing to the day 0 samples (which contained 1×10^6 ASCs).

2.3.3 Growth Factor Release Kinetics—The growth factor release kinetics from the HBDS/nanofiber layered scaffold were determined *in vitro* as described previously for HBDS alone [7, 8, 10]. Eleven-layer scaffolds (i.e., 6 layers of PLGA and 5 layers of fibrin, dimensions: 7×3×1 mm) containing 50 ng of PDGF-BB (10 μg/mL, human-derived, R&D Systems, per scaffold) were made with and without the HBDS (N=4). Scaffolds lacking the HBDS consisted of PLGA nanofiber mats layered with fibrin; these were identical to the HBDS, but lacked the heparin component. HBDS gels and fibrin gels were also made as controls (N=4-6). The total amount of HBDS or fibrin was 30 μL per scaffold. After

polymerization, the scaffolds were placed in the bottom of a 1.5 mL microcentrifuge tube and an equivalent amount of PBS (30 μL) was added on top of each sample. All 30 μl were collected daily and replaced with fresh PBS. All of the collected solutions were stored at -80°C. On day 9, any remaining growth factor in the scaffolds and gels was extracted as previously described [7, 8, 10]. An enzyme-linked immunosorbent assay (ELISA) for PDGF-BB (R&D Systems, MN) was performed on all collected solutions (including the extraction samples) according to the manufacturer's instructions. The cumulative percentage of PDGF-BB released from each of the delivery systems (i.e. fibrin, HBDS, fibrin/nanofiber layered scaffold, HBDS/nanofiber layered scaffold) was plotted over time for comparison.

2.4 In vivo studies

2.4.1 Flexor tendon animal model—All procedures were approved by the Washington University Animal Studies Committee. A series of surgeries were performed in order to: (1) ensure that the scaffold did not elicit a negative inflammatory response, (2) determine cell viability, and (3) determine the early degradation of the scaffold after implantation. Prior to cell seeding and assembly of the scaffolds, ASCs were labeled with a fluorescent membrane dye (Di-I, Invitrogen) according to the manufacturer's instructions. Flexor tendon injury and repair was performed in the clinically relevant canine animal model (N=15) using surgical techniques identical to those used in humans [6, 7, 9, 14, 31, 32]. Eleven-layer scaffolds (dimensions: 7×3×1 mm), either containing 1×10^6 autologous ASCs (isolated 7 day prior) or left acellular, were implanted into the intrasynovial flexor tendons of adult mongrel dogs (20-30kg, Covance, Denver, Pennsylvania) at the time of repair as follows (Figure 3). The sheaths of the second and fifth digits of the right forelimb in the region between the annular pulleys proximal and distal to the proximal interphalangeal joint were exposed through midlateral incisions. The sheaths were entered and the flexor digitorum profundus tendons were transected sharply. Longitudinally oriented horizontal slits were created in the center of each tendon stump for scaffold implantation. The HBDS/nanofiber scaffold was secured within the repair site using a core suture (4-0 Supramid) and sealed in that location using a running epitenon suture (6-0 Proline). Each canine received one cellular and one acellular scaffold or one acellular and one naive repair in either the second or fifth digit. After surgery, the operated-on right forelimb was immobilized using a fiberglass shoulder spica cast with the elbow flexed to 90° and the wrist flexed to 70°. To mimic the typical clinical post-operative rehabilitation protocol, controlled passive motion was applied to the digits during two five-minute rehabilitation sessions performed five days a week starting on the first postoperative day [33, 34]. The dogs were euthanized at 3 or 9 days post-operatively. The operated tendons was removed by dissection and prepped for either gene expression analysis at 3 days (N=4), histologic analysis at 9 days (N=6; 3 for immunofluorescent imaging and 3 for evaluation of biocompatibility), and total DNA analysis at 9 days (N=5). Adhesion formation between the tendon and its sheath was qualitatively evaluated at the time of dissection. Tendons from the contralateral paw were also dissected to serve as normal/uninjured controls. A subset of scaffolds (n=3) was prepared with a small amount of fluorescein isothiocyanate (FITC, 1.85 μg per scaffold) incorporated into the PLGA during fabrication. These scaffolds were prepared in order to identify the scaffold 9 days post-operatively using fluorescent imaging of histologic sections. A "time-zero" control was also performed on a cadaver animal to assess the scaffold structure and cellularity at the time of implantation.

2.4.2 Histology—Upon dissection, adhesion formation was assessed qualitatively. It was noted whether any adhesions were present, and if so, whether they were mild or severe. Tendons allocated for histology were fixed in 4% paraformaldehyde overnight, frozen in Optimal Cutting Temperature Compound (Tissue-Tek CRYO-OCT, Fisher Scientific), and cut into 5 μm sections. The residence time of the scaffold and the viability of the implanted

cells were examined using a fluorescent microscope equipped with the appropriate filters. To examine the immune response at the periphery of the scaffold, sections were stained with hematoxylin and eosin (H&E) and assessed for various immune cells (i.e., polymorphonuclear cells (PMNs) and monocytes) by an independent certified pathologist (NH), blinded to group. However, despite blinding, we note that the scaffold was apparent in some sections. Fibroblasts were characterized as spindle-shaped cells with an elliptic nucleus and thin cytoplasm. PMNs were identified as cells containing nuclei with two to four lobules and a granulated cytoplasm while cells with single-lobed or kidney-shaped nuclei were classified as monocytes. Apoptotic cells were characterized by nuclear fragmentation and condensation. A standard scoring system was used to determine the levels of each outcome (- no prevalence, + mild prevalence, ++ moderate prevalence, +++ marked prevalence). For overall cellularity and the prevalence of certain cell types, the number of cells per high powered field (HPF, 20×) was counted and assigned a score as follows: + <50 per HPF, ++ 51-100 per HPF, +++ 101-150 per HPF, ++++ >150 per HPF. Apoptosis and vascularity were measured on the following scale: + <5 per HPF, ++ 6-10 per HPF, +++ > 10 per HPF. All assessments were done using a 20× objective and 5-8 fields of view were averaged. Sections were also stained with Picrosirius Red for collagen alignment and viewed under polarized light. The analysis focused on the tissue adjacent to the scaffold.

2.4.3 Quantitative Real-time PCR—Tendons allocated for gene expression were dissected and 10 mm sections (5 mm on each side of the repair) were isolated and immediately flash frozen in liquid nitrogen. RNA was extracted from the tendons using the RNeasy mini kit (Qiagen, CA) following the manufacturer's protocol. RNA yield was quantified using a NanoDrop spectrophotometer (Thermo Scientific, DE) and 500 ng of RNA was reverse transcribed to cDNA using the Superscript VILO cDNA synthesis kit (Invitrogen Corporation, CA) following manufacturer's instructions. Real time PCR reactions were performed using SYBR Green chemistry on a StepOnePlus Real-Time PCR System (Applied Biosystems, CA). All primers for real-time PCR were purchased (Qiagen, CA). Gene expression changes were measured for the inflammation-related genes tumor necrosis factor alpha (TNF-alpha), interleukin 1 beta (IL1-beta), nitric oxide synthase 2A (Nos2A), and cyclooxygenase 2 (COX-2), and matrix remodeling-related genes metalloproteinase 1, 3, 13 (MMP-1, MMP-3, MMP-13, respectively). Results were expressed as fold change relative to the housekeeping gene glyceraldehyde 3-phosphate dehydrogenase (GAPDH).

2.4.4 Total DNA Content—Tendons allocated for Total DNA Content (N=5) were dissected and 10 mm sections (5 mm on each side of the repair) were isolated. The tendon samples were digested with papain and DNA content was determined fluorometrically with use of a PicoGreen assay kit (Invitrogen, CA). The results were normalized to the dry weight of the tendon sample.

2.5 Statistics

Cell viability within the scaffolds over time was assessed using paired t-tests to compare absorbance values at each timepoint and the values obtained on day 0. To compare growth factor release among the HBDS/nanofiber scaffold, HBDS alone, fibrin alone, and fibrin/nanofiber scaffold groups, a multi-factor ANOVA (for group and time) was performed. For simplicity and clarity, significance is only presented for the endpoint values (i.e., day 9 values). To determine the effect of the HBDS/nanofiber on inflammation- and matrix remodeling-related gene expression, mean Ct values were compared using an ANOVA (groups: acellular, naive repair, normal) followed by a least squared differences post-hoc test when the ANOVA showed a significant effect. A paired t-test was also performed on the Ct values of GAPDH to ensure the consistency of our housekeeping gene ($p > 0.05$). Samples

from the same animal were treated in a paired fashion to account for animal-to-animal variances. The total DNA content was compared between cellular, acellular, and uninjured groups using an ANOVA. Significance for all statistical analyses was set to $p < 0.05$.

3. RESULTS

3.1 Cells remain viable in the HBDS/nanofiber scaffold *in vitro*

The number of cells within the scaffolds remained approximately constant for up to 14 days *in vitro*, with no statistically significant changes over time (Figure 4A). The percentage of viable cells on day 14 compared to day 0 was approximately 81%. Stable cell numbers over time could result from maintenance of non-proliferating cells or a balance between proliferating, migrating, and apoptotic cells, resulting in a zero-sum outcome. Migration of cells out of the scaffold and onto the plastic of the wells was indeed observed. Migration of cells out of the scaffold in the *in vivo* setting may allow the cells to incorporate into the adjacent tendon tissue and produce new extracellular matrix. A type II statistical error cannot be ruled out for the non-significant cell number outcome; a post hoc power analysis revealed that 14-18 samples would be required to detect a statistically significant difference for the effect size seen (i.e., a 15% increase in viability at day 1 or 13-26% decreases in viability at days 3 – 14).

3.2 Sustained delivery of PDGF-BB was achieved from the HBDS/nanofiber scaffold

Sustained delivery of PDGF-BB was achieved from the HBDS/Nanofiber scaffold (Figure 4B). The HBDS/nanofiber scaffold released an initial burst of growth factor amounting to ~22% of the total dosage on the first day. The remaining growth factor was released slowly over the course of the next 8 days, with a total release of ~71% by day 9. The fibrin/nanofiber scaffold, which did not contain the heparin-binding delivery system, released a similar initial burst of growth factor (~28%), but released more growth factor thereafter, for a total release of ~88% by day 9. The fibrin alone released the greatest initial burst (~40%) and released nearly all of the growth factor (~97%) by 9 days. Surprisingly, the HBDS alone released the least growth factor overall over the studied time period, with a total release of only 46%. Total release at 9 days was significantly different among all groups (Figure 4B).

3.3 The HBDS/nanofiber scaffolds were well-tolerated in the *in vivo* flexor tendon repair setting

Based on gross observations at the time of dissection, the HBDS/nanofiber scaffold did not elicit any negative responses. The tendons were intact and had minimal adhesions at the repair site (Figure 5D). Out of 7 naive repairs, 5 had no adhesions, 2 had mild adhesions, and 0 had severe adhesions. Out of 7 repairs that received scaffolds, 5 had no adhesions, 1 had mild adhesions, and 1 had severe adhesions. Histological analysis showed a mild influx of immune cells (i.e., polymorphonuclear cells and monocytes) around the implanted scaffolds 9 days post-operatively (Figure 5, Table 1). Overall cellularity was increased in the group that received the scaffold, including increases in polymorphonuclear cells and monocytes. A small increase in apoptotic cells was also observed and was related to the increased presence of polymorphonuclear cells. No significant difference was noted for vascular profiles between the two groups. Similarly, there were no statistically significant changes when comparing quantitative real-time PCR results for repairs that received acellular scaffolds to naive repairs (Figure 6). For certain genes, a type II statistical error was possible when comparing expression in the acellular scaffold group to expression in the naïve repair group. Based on a post-study power analysis: N=24 would be required to show that TNF-alpha was significantly higher in the naive repair group, N=28 would be required to show that COX2 was significantly higher in the scaffold group, N=39 would be required to show that MMP3 was significantly higher in the scaffold group, and N=14 would be

required to show that MMP3 was significantly higher in the scaffold group. As expected both repair groups showed a significant upregulation in gene expression relative to uninjured controls (Figure 6). Using fluorescent labeling and imaging techniques, the scaffold was identifiable at the repair site 9 days post-operatively, indicating a slow degradation rate relative to the time-course of tendon healing (Figure 2E).

3.4 Successful delivery of ASCs was achieved *in vivo* using the HBDS/nanofiber scaffolds

Fluorescent imaging verified the viability of the implanted cells 9 days post-operatively. Co-localization of the membrane dye (Di-I) and the nuclear stain (Hoescht 33258) were evident in the time zero and 9 day cellular groups, but not in the 9 day acellular group (Figure 7A-C). In support of the qualitative fluorescent imaging, there was a significant increase in total DNA content in the cellular group compared to the acellular group and normal/uninjured controls (Figure 7D). While there is a significant increase in the total DNA of the cellular group, the DNA assay does not distinguish between cell types. We cannot determine, therefore, whether that increase was due to the implanted ASCs or infiltration of additional cells (via a chemotactic mechanism initiated by the ASCs). Moreover, the comparison between the uninjured group and acellular group indicates that the scaffold alone attracts host cells, however, neither the origin nor phenotype (e.g., inflammatory vs. fibroblastic) of these cells could be determined.

4. DISCUSSION

Flexor tendon healing often fails due to the paucity of native cells available to mount a repair response. For example, flexor tendon healing depends on cell migration from the tendon's surface layer and digital sheath to the repair site, cell proliferation between the tendon stumps, and ECM synthesis by tendon fibroblasts [35-37]. However, these processes are inherently slow in the hypocellular environment of many tendons. In an effort to enhance cell activity, we previously administered the growth factors PDGF-BB and basic fibroblast growth factor (bFGF) at the time of tendon repair in a canine model [6, 7, 9, 14]. Although both factors stimulated cellular activity, neither enhanced repair site strength. We conclude that due to a paucity of tendon fibroblasts, growth factor application by itself was insufficient to stimulate biomechanical changes in the repair process by a significant amount. Flexor tendon healing will remain problematic unless two fundamental issues are addressed: (1) the relatively low number of tendon fibroblasts at the repair site and (2) the slow rate of ECM synthesis.

Cell-based therapies can directly address these issues; prior studies support the use of stem cells to enhance healing after extrasynovial tendon [38-42], articular cartilage [43-45], and myocardial [46-50] repair. Omae *et al* examined the potential for a decellularized xenotendon combined with bone marrow stromal cells to enhance patellar tendon defect healing in a rabbit model [38]. Decellularized tendons were sectioned, seeded with stromal cells, bundled into composites, and implanted into patellar tendon defects. Histologic and gene expression outcomes indicated that cells remained viable after implantation, expressed a tendon fibroblast phenotype, and enhanced tendon metabolism. Further, a recent *in vitro* study suggested that combining bone marrow stromal cells with a growth factor may be a beneficial approach for flexor tendon repair [51]. Despite these promising results in multiple tissues, there are no reports where a combined cell and growth factor therapy has been used to repair paucicellular intrasynovial flexor tendons in a clinically relevant animal model.

In the current study, we presented an innovative, layered scaffold design that combined the cell and growth factor delivery capabilities of a HBDS and the structural integrity of a PLGA nanofiber mat. The layered design allows for modularity; the size of the scaffold can be tailored to the specific tendon application, and the cell and growth factor delivery can be

controlled. The HBDS is also highly versatile, allowing for the delivery of any heparin-binding growth factor. This new scaffold design improved on the previously described HBDS scaffold [6, 7, 9, 14], which successfully delivered growth factors at a sustained rate, but was difficult to handle surgically due to its hydrogel consistency. Importantly, the current study showed that layering the HBDS with PLGA nanofiber mats did not disrupt the controlled delivery capabilities of the HBDS. *In vivo* studies in a clinically relevant large animal study demonstrated that the delivered ASCs remained viable for at least 9 days post-operatively. Furthermore, histological and gene expression outcomes from the animal model demonstrated that the scaffold was biocompatible up to 9 days in the relevant tendon healing setting.

Sustained growth factor release was also achieved with the scaffold. We used PDGF-BB in this study as a model growth factor for delivery and tendon repair. We expected the HBDS/nanofiber scaffold to have the slowest release rate among the groups tested. Theoretically, the HBDS/nanofiber scaffold should retain the growth factor both by affinity to heparin and diffusion limitations resulting from the nanofiber mat and the layered scaffold design. In contrast, the HBDS retains the growth factor by heparin affinity alone. While the mechanism of faster release from the HBDS/nanofiber scaffold compared to the HBDS alone is unknown, we speculate that the higher surface area in the thin rectangular HBDS layers in the HBDS/nanofiber scaffold compared to the bulk HBDS gel may explain this result. Nevertheless, our intent was to show that the scaffold could deliver both cells and growth factors simultaneously without adverse reactions. Future studies will further investigate the release kinetics and biologic effects of various growth factors for improving flexor tendon healing.

A number of questions must be resolved before the scaffold presented here can be used clinically. First, an effective growth factor and dosage will need to be chosen. While the natural wound healing response is complex and involves a cascade of carefully timed growth factor profiles, this natural process typically leads to scar-mediated healing and adhesions in most tendon and ligament repair settings, and in flexor tendon repair in particular. Our approach is to take a systematic and simplified approach to enhance healing. In this manner, we can isolate the effect of each growth factor delivered to inform the next, potentially combinatorial, approach. Based on previous studies, we hypothesize that PDGF-BB would enhance flexor tendon repair [6, 7, 9] and ASC proliferation [52-54], with little effect on ASC differentiation. Other growth factors (such as the tenogenic bone morphogenetic protein 12 [24, 25, 55]) can also be examined. These studies will determine the long-term effects of this scaffold on tendon healing, and the potential for ASCs and growth factors to enhance the biomechanical properties of repaired flexor tendons *in vivo*.

Second, flexor tendon function depends on gliding of the tendon within its sheath; adhesion formation after repair can significantly impair this function. It is possible that the administration of growth factors and/or ASCs will stimulate the formation of adhesions extending from the digital sheath to the tendon surface. This outcome was observed when bFGF was delivered with a HBDS to tendon repairs in our previous study [14]. However, the potential anti-inflammatory effects of ASCs [20-22], coupled with the use of early controlled passive mobilization [34], reduces the possibility of this adverse outcome.

Third, although data in the current study indicate that the scaffold is well-tolerated *in vivo*, there is a chance that the PLGA will incite a negative reaction under some conditions. The scaffold did attract a small number of polymorphonuclear cells and monocytes, which led to a mild increase in apoptosis. Moreover, MMP and COX-2 gene expression in the scaffold group were increased, on average, in the current study compared to the naïve repair group. These increases, however, were not statistically significant.

Finally, we tracked implanted ASCs using a membrane dye. Although this dye will label cells, it does not indicate whether the cells are alive. The same limitation applies to the total DNA assay, which will label DNA regardless of cell viability. Co-localization of the membrane dye with a nuclear dye (see inset of figure 7B) provides evidence that the implanted ASCs were viable at 9 days. However, further analyses (e.g., using a TUNEL assay) are needed to conclusively show that implanted cells remain viable throughout the tendon healing process.

The relatively small sample size and the high variability in our gene expression data may have resulted in a type II statistical error (i.e., a false negative). Importantly, when examining inflammatory factors, TNF-alpha was decreased and IL1-beta was unchanged in the scaffold group compared to the naïve repair group. As with the other genes, the differences between the two repair groups were not statistically significant. Due to ethical and cost consideration associated with a large animal model, we determined that it would be inappropriate to increase the sample size such that a power of 80% was achieved; this would require N=14-39 for the four genes where a type II error was likeliest. In the case that a negative response is seen with the current scaffold materials, alternative polymer formulations can be electrospun to form the nanofiber mat layers of the scaffold (e.g., collagen, poly(*ε*-caprolactone) (PCL), poly(L-lactic) acid (PLA)).

In conclusion, a novel scaffold was developed to concurrently deliver PDGF-BB and ASCs to a tendon repair site. *In vitro* studies verified that the cells remained viable and that sustained growth factor release was achieved. *In vivo* studies in a large animal tendon model verified that the approach was clinically relevant and that the cells remained viable in the tendon repair environment. Specifically, no negative reaction was seen grossly at dissection or at the mRNA level; only a mild immune response was detected histologically, viable ASCs were found at the repair site 9 days postoperatively; and increased total DNA was demonstrated in ASC-treated tendons. The novel layered scaffold has the potential for improving tendon healing due to its ability to deliver both cells and growth factors simultaneously in a surgically convenient manner.

Acknowledgments

The study was funded by the National Institutes of Health (R01-AR060820, R01-AR062947). Histologic processing was performed by the Musculoskeletal Research Center at Washington University, supported by grant P30-AR057235 from the National Institutes of Health. The authors thank Dr. Jim Ross for creating the schematics of the scaffold and the repair technique. The authors thank Drs. David Amiel and Fred Harwood for performing the total DNA assay.

References

1. de Putter CE, Selles RW, Polinder S, Panneman MJ, Hovius SE, van Beeck EF. Economic impact of hand and wrist injuries: health-care costs and productivity costs in a population-based study. J Bone Joint Surg Am. 2012; 94:e56. [PubMed: 22552678]
2. Feuerstein M, Miller VL, Burrell LM, Berger R. Occupational upper extremity disorders in the federal workforce. Prevalence, health care expenditures, and patterns of work disability. J Occup Environ Med. 1998; 40:546–55. [PubMed: 9636935]
3. Kelsey, JL. New York, NY: Churchill Livingstone; 1997. Upper extremity disorders: frequency, impact and cost.
4. Kreiger N, Kelsey JL, Harris C, Pastides H. Injuries to the upper extremity: patterns of occurrence. Clin Plast Surg. 1981; 8:13–9. [PubMed: 7273612]
5. Thomopoulos S, Harwood FL, Silva MJ, Amiel D, Gelberman RH. Effect of several growth factors on canine flexor tendon fibroblast proliferation and collagen synthesis in vitro. J Hand Surg [Am]. 2005; 30:441–7.

6. Gelberman RH, Thomopoulos S, Sakiyama-Elbert SE, Das R, Silva MJ. The early effects of sustained platelet-derived growth factor administration on the functional and structural properties of repaired intrasynovial flexor tendons: an in vivo biomechanic study at 3 weeks in canines. J Hand Surg [Am]. 2007; 32:373–9.
7. Thomopoulos S, Zaegel M, Das R, Harwood FL, Silva MJ, Amiel D, et al. PDGF-BB released in tendon repair using a novel delivery system promotes cell proliferation and collagen remodeling. J Orthop Res. 2007; 25:1358–68. [PubMed: 17551975]
8. Sakiyama-Elbert SE, Das R, Gelberman RH, Harwood F, Amiel D, Thomopoulos S. Controlled-release kinetics and biologic activity of platelet-derived growth factor- BB for use in flexor tendon repair. J Hand Surg [Am]. 2008; 33:1548–57.
9. Thomopoulos S, Das R, Silva MJ, Sakiyama-Elbert S, Harwood FL, Zampiakis E, et al. Enhanced flexor tendon healing through controlled delivery of PDGF-BB. J Orthop Res. 2009; 27:1209–15. [PubMed: 19322789]
10. Thomopoulos S, Das R, Sakiyama-Elbert S, Silva MJ, Charlton N, Gelberman RH. bFGF and PDGF-BB for tendon repair: controlled release and biologic activity by tendon fibroblasts in vitro. Ann Biomed Eng. 2010; 38:225–34. [PubMed: 19937274]
11. Lou J, Tu Y, Burns M, Silva MJ, Manske P. BMP-12 gene transfer augmentation of lacerated tendon repair. J Orthop Res. 2001; 19:1199–202. [PubMed: 11781024]
12. Hamada Y, Katoh S, Hibino N, Kosaka H, Hamada D, Yasui N. Effects of monofilament nylon coated with basic fibroblast growth factor on endogenous intrasynovial flexor tendon healing. J Hand Surg [Am]. 2006; 31:530–40.
13. Tang JB, Cao Y, Zhu B, Xin KQ, Wang XT, Liu PY. Adeno-associated virus-2-mediated bFGF gene transfer to digital flexor tendons significantly increases healing strength. an in vivo study. J Bone Joint Surg Am. 2008; 90:1078–89. [PubMed: 18451401]
14. Thomopoulos S, Kim HM, Das R, Silva MJ, Sakiyama-Elbert S, Amiel D, et al. The effects of exogenous basic fibroblast growth factor on intrasynovial flexor tendon healing in a canine model. J Bone Joint Surg Am. 2010; 92:2285–93. [PubMed: 20926722]
15. Sakiyama-Elbert SE, Hubbell JA. Development of fibrin derivatives for controlled release of heparin-binding growth factors. Journal of Controlled Release. 2000; 65:389–402. [PubMed: 10699297]
16. Lu L, Peter SJ, Lyman MD, Lai HL, Leite SM, Tamada JA, et al. In vitro and in vivo degradation of porous poly(DL-lactic-co-glycolic acid) foams. Biomaterials. 2000; 21:1837–45. [PubMed: 10919687]
17. Nair LS, Laurencin CT. Biodegradable polymers as biomaterials. Progress in Polymer Science. 2007; 32:762–98.
18. Gimble JM. Adipose tissue-derived therapeutics. Expert Opin Biol Ther. 2003; 3:705–13. [PubMed: 12880371]
19. Gimble JM, Katz AJ, Bunnell BA. Adipose-derived stem cells for regenerative medicine. Circ Res. 2007; 100:1249–60. [PubMed: 17495232]
20. Niemeyer P, Kornacker M, Mehlhorn A, Seckinger A, Vohrer J, Schmal H, et al. Comparison of immunological properties of bone marrow stromal cells and adipose tissue-derived stem cells before and after osteogenic differentiation in vitro. Tissue Eng. 2007; 13:111–21. [PubMed: 17518585]
21. Fang B, Song Y, Liao L, Zhang Y, Zhao RC. Favorable response to human adipose tissue-derived mesenchymal stem cells in steroid-refractory acute graft-versus-host disease. Transplant Proc. 2007; 39:3358–62. [PubMed: 18089385]
22. Yanez R, Lamana ML, Garcia-Castro J, Colmenero I, Ramirez M, Bueren JA. Adipose tissue-derived mesenchymal stem cells have in vivo immunosuppressive properties applicable for the control of the graft-versus-host disease. Stem Cells. 2006; 24:2582–91. [PubMed: 16873762]
23. Vieira NM, Brandalise V, Zucconi E, Secco M, Strauss BE, Zatz M. Isolation, characterization, and differentiation potential of canine adipose-derived stem cells. Cell Transplant. 2010; 19:279–89. [PubMed: 19995482]

24. Park A, Hogan MV, Kesturu GS, James R, Balian G, Chhabra AB. Adipose-Derived Mesenchymal Stem Cells Treated with Growth Differentiation Factor-5 Express Tendon-Specific Markers. Tissue Eng Part A. 2010; 16:2941–51. [PubMed: 20575691]
25. James R, Kumbar SG, Laurencin CT, Balian G, Chhabra AB. Tendon tissue engineering: adipose-derived stem cell and GDF-5 mediated regeneration using electrospun matrix systems. Biomed Mater. 2011; 6:025011. [PubMed: 21436509]
26. Ramchandani M, Pankaskie M, Robinson D. The influence of manufacturing procedure on the degradation of poly(lactide-co-glycolide) 85:15 and 50:50 implants. Journal of Controlled Release. 1997; 43:161–73.
27. Katta P, Alessandro M, Ramsier RD. Continuous electrospinning of aligned polymer nanofibers onto a wire drum collector. Nano Letters. 2004; 4:2215–8.
28. Liu W, Thomopoulos S, Xia Y. Electrospun nanofibers for regenerative medicine. Advanced Healthcare Materials. 2012; 1:10–25. [PubMed: 23184683]
29. Martinello T, Bronzini I, Maccatrozzo L, Mollo A, Sampaolesi M, Mascarello F, et al. Canine adipose-derived-mesenchymal stem cells do not lose stem features after a long-term cryopreservation. Research in veterinary science. 2011; 91:18–24. [PubMed: 20732703]
30. Priya N, Sarcar S, Majumdar AS, Sundarraj S. Explant culture: a simple, reproducible, efficient and economic technique for isolation of mesenchymal stromal cells from human adipose tissue and lipoaspirate. Journal of tissue engineering and regenerative medicine. 2012:1–9. [PubMed: 22837175]
31. Potenza AD. Detailed evaluation of healing processes in canine flexor digital tendons. Mil Med. 1962; 127:34–47. [PubMed: 14488262]
32. Kim HM, Nelson G, Thomopoulos S, Silva MJ, Das R, Gelberman RH. Technical and biological modifications for enhanced flexor tendon repair. J Hand Surg Am. 2010; 35:1031–7. quiz 8. [PubMed: 20513584]
33. Gelberman RH, Amiel D, Gonsalves M, Woo S, Akeson WH. The influence of protected passive mobilization on the healing of flexor tendons: a biochemical and microangiographic study. Hand. 1981; 13:120–8. [PubMed: 7286796]
34. Boyer MI, Goldfarb CA, Gelberman RH. Recent progress in flexor tendon healing. The modulation of tendon healing with rehabilitation variables. J Hand Ther. 2005; 18:80–5. quiz 6. [PubMed: 15891963]
35. Gelberman RH, Khabie V, Cahill CJ. The revascularization of healing flexor tendons in the digital sheath. A vascular injection study in dogs. J Bone Joint Surg Am. 1991; 73:868–81. [PubMed: 1712787]
36. Gelberman RH, Amiel D, Harwood F. Genetic expression for type I procollagen in the early stages of flexor tendon healing. Journal of Hand Surgery - American. 1992; 17:551–8.
37. Gelberman RH, Steinberg D, Amiel D, Akeson W. Fibroblast chemotaxis after tendon repair. J Hand Surg [Am]. 1991; 16:686–93.
38. Omae H, Sun YL, An KN, Amadio PC, Zhao C. Engineered tendon with decellularized xenotendon slices and bone marrow stromal cells: an in vivo animal study. Journal of tissue engineering and regenerative medicine. 2012; 6:238–44. [PubMed: 21449044]
39. Gulotta LV, Kovacevic D, Packer JD, Deng XH, Rodeo SA. Bone marrow-derived mesenchymal stem cells transduced with scleraxis improve rotator cuff healing in a rat model. Am J Sports Med. 2011; 39:1282–9. [PubMed: 21335341]
40. Young RG, Butler DL, Weber W, Caplan AI, Gordon SL, Fink DJ. Use of mesenchymal stem cells in a collagen matrix for Achilles tendon repair. Journal of Orthopaedic Research. 1998; 16:406–13. [PubMed: 9747780]
41. Awad HA, Boivin GP, Dressler MR, Smith FN, Young RG, Butler DL. Repair of patellar tendon injuries using a cell-collagen composite. Journal of Orthopaedic Research. 2003; 21:420–31. [PubMed: 12706014]
42. Gulotta LV, Kovacevic D, Montgomery S, Ehteshami JR, Packer JD, Rodeo SA. Stem cells genetically modified with the developmental gene MT1-MMP improve regeneration of the supraspinatus tendon-to-bone insertion site. Am J Sports Med. 2010; 38:1429–37. [PubMed: 20400753]

43. Tang QO, Carasco CF, Gamie Z, Korres N, Mantalaris A, Tsiridis E. Preclinical and clinical data for the use of mesenchymal stem cells in articular cartilage tissue engineering. Expert Opin Biol Ther. 2012; 12:1361–82. [PubMed: 22784026]
44. Huselstein C, Li Y, He X. Mesenchymal stem cells for cartilage engineering. Biomed Mater Eng. 2012; 22:69–80. [PubMed: 22766704]
45. van Osch GJ, Brittberg M, Dennis JE, Bastiaansen-Jenniskens YM, Erben RG, Konttinen YT, et al. Cartilage repair: past and future--lessons for regenerative medicine. J Cell Mol Med. 2009; 13:792–810. [PubMed: 19453519]
46. Joggerst SJ, Hatzopoulos AK. Stem cell therapy for cardiac repair: benefits and barriers. Expert Rev Mol Med. 2009; 11:e20. [PubMed: 19586557]
47. Nesselmann C, Ma N, Bieback K, Wagner W, Ho A, Konttinen YT, Zhang H, Hinscu M, Steinhoff G. Mesenchymal stem cells and cardiac repair. J Cell Mol Med. 2008; 12:1795–810. [PubMed: 18684237]
48. Ramos GA, Hare JM. Cardiac cell-based therapy: cell types and mechanisms of actions. Cell Transplant. 2007; 16:951–61. [PubMed: 18293894]
49. Mathiasen AB, Haack-Sorensen M, Kastrup J. Mesenchymal stromal cells for cardiovascular repair: current status and future challenges. Future Cardiol. 2009; 5:605–17. [PubMed: 19886787]
50. Yamahara K, Nagaya N. Stem cell implantation for myocardial disorders. Curr Drug Deliv. 2008; 5:224–9. [PubMed: 18673267]
51. Hayashi M, Zhao C, Amadio PC. The effects of growth and differentiation factor 5 on bone marrow stromal cell transplants in an in vitro tendon healing model. J Hand Surg [Eur]. 2011; 36:271–9.
52. Qiu P, Song W, Niu Z, Bai Y, Li W, Pan S, Peng S, Hua J. Platelet-derived growth factor promotes the proliferation of human umbilical cord-derived mesenchymal stem cells. Cell Biochem Funct. 2012 [Epub ahead of print].
53. Kilian O, Flesch I, Wenisch S, Taborski B, Jork A, Schnettler R, et al. Effects of platelet growth factors on human mesenchymal stem cells and human endothelial cells in vitro. Eur J Med Res. 2004; 9:337–44. [PubMed: 15337634]
54. Pountos I, Georgouli T, Henshaw K, Bird H, Jones E, Giannoudis PV. The effect of bone morphogenetic protein-2, bone morphogenetic protein-7, parathyroid hormone, and platelet-derived growth factor on the proliferation and osteogenic differentiation of mesenchymal stem cells derived from osteoporotic bone. J Orthop Trauma. 2010; 24:552–6. [PubMed: 20736793]
55. Wolfman NM, Hattersley G, Cox K, Celeste AJ, Nelson R, Yamaji N, et al. Ectopic induction of tendon and ligament in rats by growth and differentiation factors 5, 6, and 7, members of the TGF-beta gene family. Journal of Clinical Investigation. 1997; 100:321–30. [PubMed: 9218508]

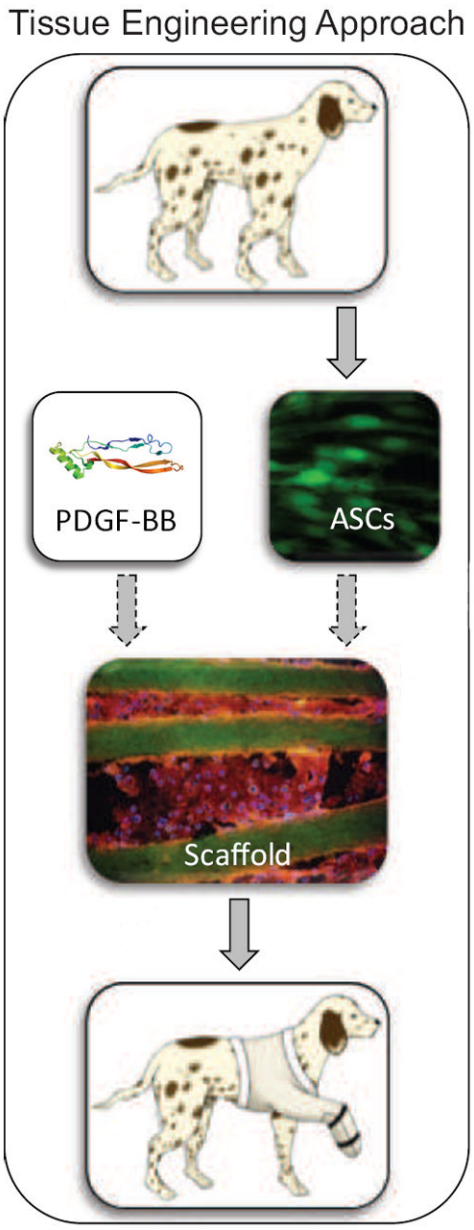

Figure 1.
Overview of the tissue engineering approach. ASCs were isolated from canine adipose tissue, combined with a growth factor (e.g., PDGF-BB), and incorporated into a layered HBDS/nanofiber scaffold. The scaffold was then implanted at the site of the flexor tendon repair, providing autologous ASCs and/or a growth factor for enhanced healing. (Dashed arrows indicates optional addition).

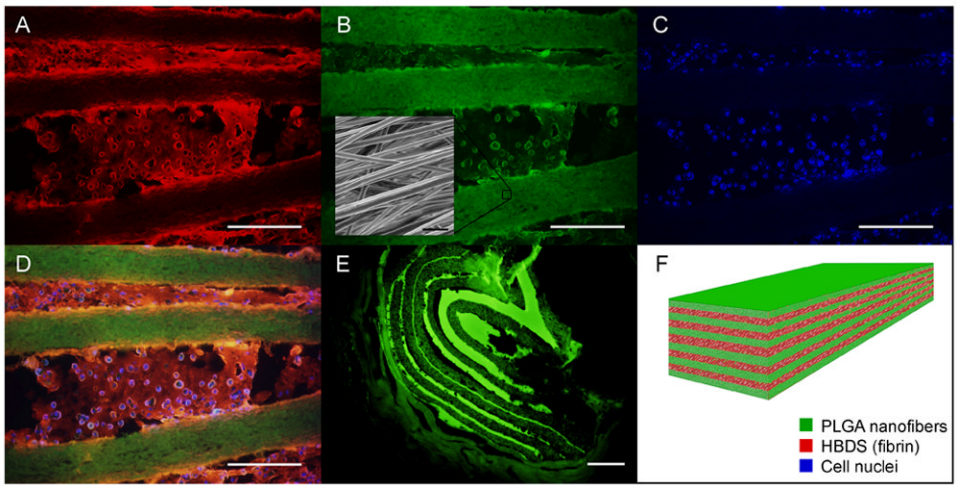

Figure 2.

A representative HBDS/nanofiber scaffold with eleven alternating layers of aligned electrospun PLGA nanofiber mats separated by HBDS containing 1×10^6 ASCs is shown. **(A-D)** Micrograph showing the HBDS/nanofiber scaffold *in vitro*; the PLGA was labelled with FITC (green), the HBDS was labeled with Alexa Fluor 546 (red), and the ASC nuclei were labeled with Hoescht 33258 (blue) (scale bar = 200 μm). **(B inset)** SEM image of the scaffold showing PLGA nanofiber alignment. **(E)** Micrograph showing the HBDS/nanofiber scaffold *in vivo* 9 days after implantation in a tendon repair. Eleven alternating layers of PLGA and HBDS can be seen (i.e., 6 layers of PLGA and 5 layers of fibrin); the PLGA was labelled with FITC (green) (scale bar = 100 μm). **(F)** A schematic of the layered scaffold is shown.

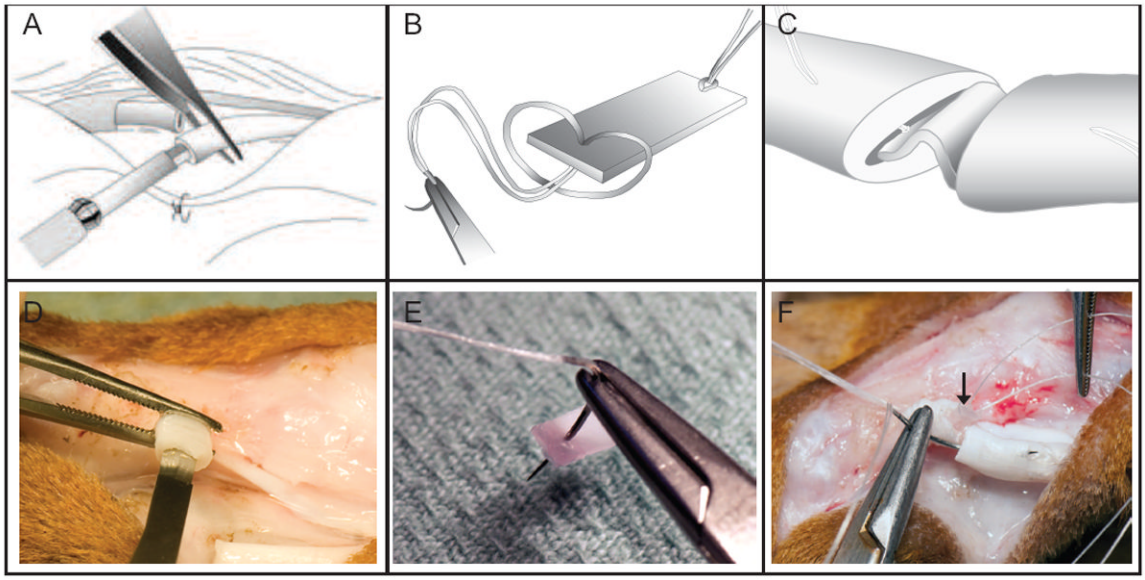

Figure 3.

A depiction of the surgical technique. **(A, D)** Flexor tendons were transected sharply and longitudinally oriented horizontal slits were created in the center of each tendon stump. **(B, E)** A HBDS/nanofiber scaffold was grasped by a core suture. **(C, F)** The scaffold was secured within the repair site.

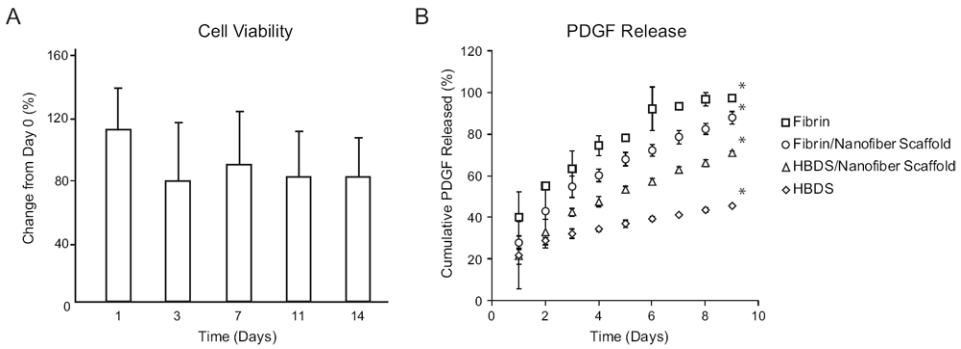

Figure 4.

(A) Cell viability within the scaffold *in vitro* compared to day 0. No significant decreases in cell viability were observed at any timepoint (1-14 days) compared to day 0 ($p \geq 0.05$, paired t-tests, N=4). **(B)** Release kinetics of PDGF-BB for the fibrin alone, the fibrin/nanofiber scaffold, the HBDS/nanofiber scaffold, and the HBDS alone. Sustained growth factor release was achieved from the HBDS/nanofiber scaffold; all groups were significantly different from each other at 9 days (* $p < 0.05$ at 9 days based on a multi-factor ANOVA; N=4-6).

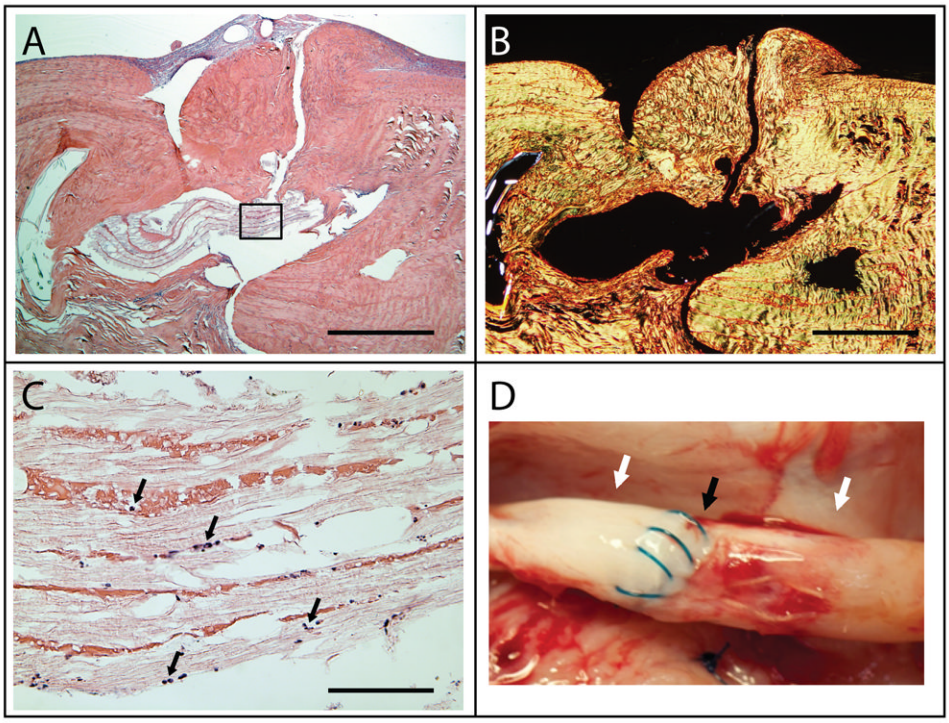

Figure 5.

(A-C) Representative histologic sections of a tendon that was repaired using an acellular HBDS/nanofiber scaffold. The sections were stained with either H&E (hematoxylin and eosin) and viewed under brightfield for cell identification (A and C) or stained with Picrosirius Red and viewed with polarized light for collagen alignment (B). No obvious inflammatory response was observed with the implantation of the scaffold 9 day post-operatively. Only a small number of immune cells infiltrated the scaffold (black arrows in C). The image in C corresponds to the black box in A. (A, B: 4× objective, 1 mm scale bar; C: 40× objective, 100 μm scale bar) **(D)** Gross observations of repaired tendons show no gapping at the repair site. A representative sample shown here demonstrates no gap (black arrow) and no adhesions between the tendon and the sheath (white arrows) 9 days post-operatively.

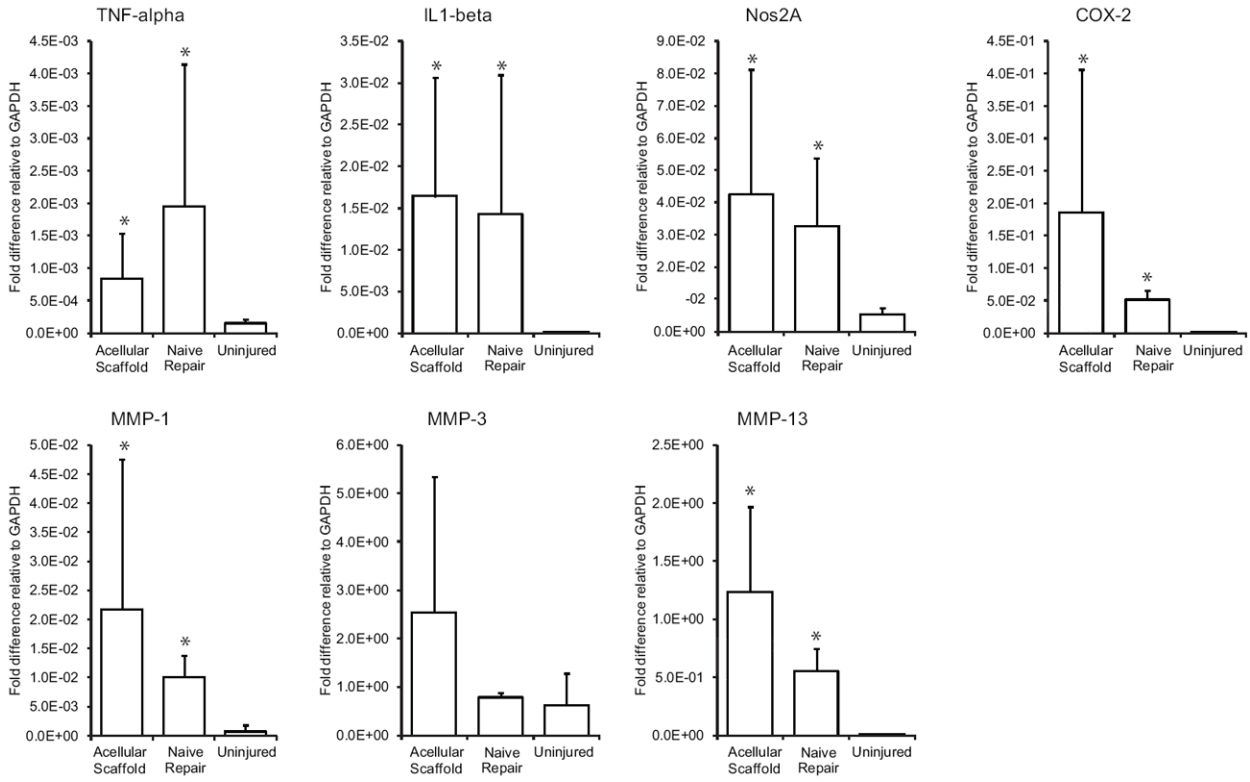

Figure 6.

Genes related to inflammation (top row) and genes related to matrix remodeling (bottom row) were significantly upregulated in the repair setting (i.e., acellular scaffold and naïve repair groups) relative to uninjured control. There were no significant differences in gene expression when comparing the acellular scaffold and naïve repair groups. (* $p < 0.05$ compared to uninjured group).

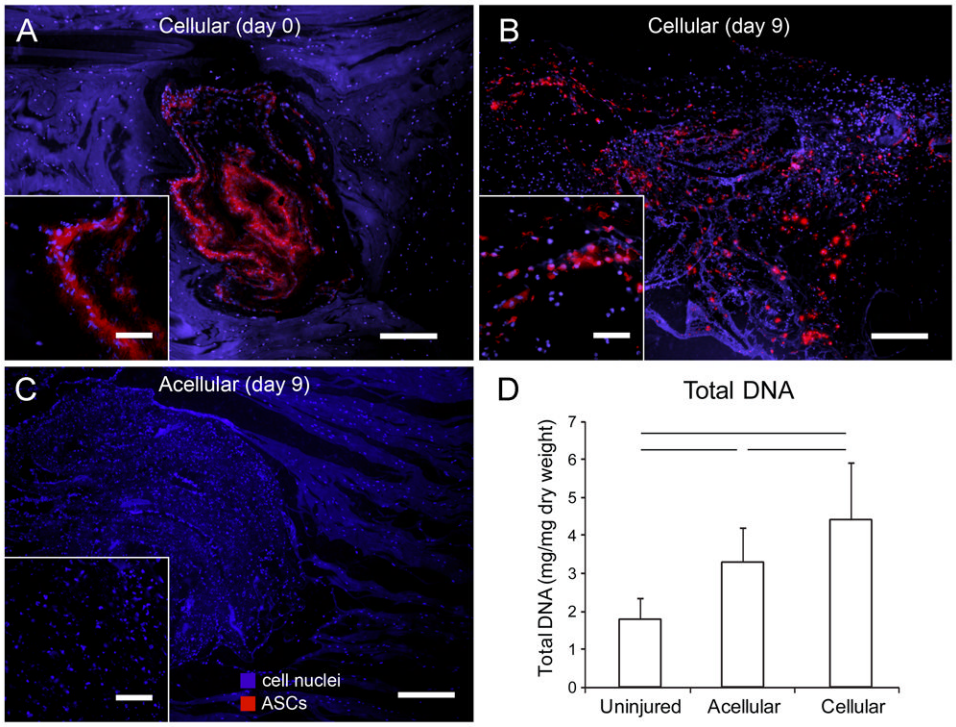

Figure 7.

(A-C) Micrographs showing the HBDS/nanofiber scaffolds at implantation (day 0) and 9 days after implantation. ASCs were labeled with the fluorescent membrane dye Di-I (red) prior to seeding. Sections were stained with Hoescht 33258 (blue) to label all cell nuclei. Co-localization of the membrane dye (red) and the nuclear stain (blue) was apparent at day 0 and 9 days after repair, indicating cell viability. An acellular scaffold is shown 9 days post-operatively for comparison. Scale bars = 200 μm for main images and 50 μm for insets. **(D)** Total DNA content in uninjured tendons, repaired tendons that received acellular scaffolds, and repaired tendons that received cellular scaffolds. (Bars signify $p<0.05$, N=5).

Table 1

Histological analysis of the immune response to the HBDS/Nanofiber scaffold 9 days post-operatively.

	Normal	Repair-Only	Scaffold
Cellularity	-	++	+
Vascularity	-	-/+	-
FB	-	+	++
PMN	-	+	++
Mono	-	++	++
Apoptosis	-	-	+

The number and type of immune cells present in tendons after implantation of an acellular scaffold was compared to those present in the repair-only and the normal/uninjured groups. A standard scoring system was used to determine the levels of each outcome (- no prevalence, + mild prevalence, ++ moderate prevalence, +++ marked prevalence). FB = foreign body, PMN = polymorphonuclear cells, Mono = monocytes (N=3).